Clustering of bacteria with heterogeneous motility

T. Vourc'h,[1,*] J. Léopoldès,[2,3,†] and H. Peerhossaini[1,4]

[1]*Laboratoire AstroParticules et Cosmologie, CNRS, Université Paris-Diderot, Université de Paris, 5 rue Thomas Mann 75013 Paris, France*

[2]*ESPCI Paris, PSL Research University, CNRS, Institut Langevin, 1 rue Jussieu, F-75005 Paris, France*

[3]*Université Paris-Est Marne-la-Vallée, 5 Bd Descartes, Champs sur Marne, Marne-la-Vallée Cedex 2, France*

[4]*Mechanics of Active Fluids Laboratory, Department of Civil and Environmental Engineering, Department of Mechanical and Materials Engineering, University of Western Ontario, London, Ontario, Canada N6A3K7*

(Received 6 September 2019; revised manuscript received 5 February 2020; accepted 5 February 2020; published 26 February 2020)

We study the clustering of a model cyanobacterium *Synechocystis* into microcolonies. The bacteria are allowed to diffuse onto surfaces of different hardness and interact with the others by aggregation and detachment. We find that soft surfaces give rise to more microcolonies than hard ones. This effect is related to the amount of heterogeneity of bacteria's dynamics as given by the proportion of motile cells. A kinetic model that emphasizes specific interactions between cells, complemented by extensive numerical simulations considering various amounts of motility, describes the experimental results adequately. The high proportion of motile cells enhances dispersion rather than aggregation.

DOI: 10.1103/PhysRevE.101.022612

I. INTRODUCTION

Divided matter tends to cluster on a wide range of length scales, depending on the range of the driving force and the type of interaction. At the molecular level, proteins aggregate in neurons as a possible mechanism for some neurodegenerative diseases [1]. Moreover, the clustering of mesoscopic phytoplankton allows vertical transport in the oceans [2] while at largest scales, the asteroid families in the main asteroid belt are believed to result from the aggregation that follows a collision [3].

Distinct from the above examples, motion in active matter such as bacteria is driven by nonequilibrium forces. The aggregation between bacterial cells in microcolonies (clusters), a fundamental step in the colonization of a surface, triggers the formation of a biofilm. This favors the adaptation of bacteria to their local environment by constituting a protective system against external toxic agents [4–9]. Biofilm formation is a major concern in health care or the food industry, but its control could also be profitable for decontamination or renewable energies.

The patterns observed following the aggregation of the cells are different from inert particles [10]. Indeed, the morphology of the biofilm reflects the complex conditions under which growth occurs, such as gradients of nutriment or light as well as number density and motility [11]. Nevertheless, some similarities exist between active cluster formation and first-order phase transitions in thermal systems [12,13].

Focusing on the dynamics at the particle scale, the balance between nucleation-division and diffusion-aggregation processes shall control the emergence of microcolonies [14–17]. For example, motility can either favor bacterial aggregation by enabling cell-cell encounters [15] but also prevent localized aggregates by enhancing dispersion [18]. Moreover, it is well known that bacteria develop several subpopulations in order to adapt to evolving environmental conditions [19], so that heterogeneous behaviors can be found inside colonies [20,21]. But how heterogeneity influences clustering in such real systems is presently unknown.

In this article, we study the growth of microcolonies of cyanobacteria *Synechocystis* on soft and hard surfaces. The latter promote higher amounts of motile bacteria p_m than the former, and the number of clusters at long times is a decreasing function of p_m. We propose that motility allows the bacteria to escape from clusters while nonmotile ones are trapped. This study highlights the necessity to account for subpopulations of variable dynamics among a given strain for an adequate description of the formation of microcolonies.

II. EXPERIMENTS

Biofilms of the wild-type strain of the cyanobacterium *Synechocystis* sp. PCC 6803 are grown for 8 days on surfaces of various hardness fixed at the bottom of the same Petri dish ("open cell"), allowing identical gas exchange and exposure to the controlled light. After introduction of the bacterial suspension in the open cell, the latter is placed into an incubator for biofilm growth. Once a day, the morphology of the various samples is imaged with a microscope. Typically, a raw image is filtered with a bandpass filter to reduce noise, before subtraction of the background, inversion and binarization. The remaining image contains a distribution of areas of contiguous pixels $\mathcal{A}_i$ which are selected based on the size of their equivalent radius $r_i = \sqrt{\mathcal{A}_i/\pi}$ compared to the radius of the bacteria r_b. All areas with $r_i < 1.4\ \mu$m, corresponding to a lower bound for the size of a *Synechocystis*, are removed from

*Present address: Physico-Chimie Curie, CNRS, Institut Curie, Paris Sciences et Lettres, 11 rue Pierre et Marie Curie 75005 Paris, France.

†julien.leopoldes@espci.fr

 ©2020 American Physical Society

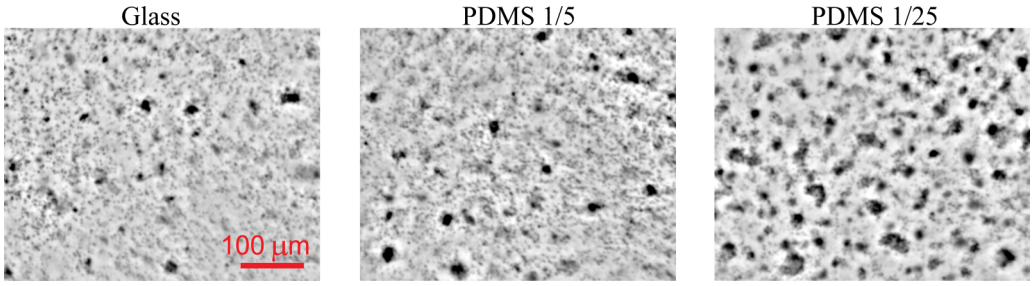

FIG. 1. Morphology of the biofilm on different substrates, 8 days after introduction of the bacteria in the cell. Glass, PDMS 1/5, and PDMS 1/25 correspond to hard, intermediate, and softer surface, respectively.

the analysis. The number of individual bacteria contained in the rest of each area is obtained from the floor function of r_i/r_b ($r_b = 2.2$ μm), which is then summed over all the areas to compute $\rho(t)$. The number of areas with $r_i > 3.1$ μm defines the number of microcolonies.

We also characterized the surface specific dynamics of bacteria in a "closed cell" with no gas exchange and designed to prevent bacteria motion due to convection [22]. In the closed cell, the use of dilute suspensions at short timescales limits the interactions between bacteria and allows the study of their individual diffusive motion, mediated by type IV pili. Video recording 1 hour after introduction of the suspension in the closed cell and subsequent particle tracking provide the measurement of the "run" and "tumble" times of the intermittent diffusion, characteristic of this system [22]. No microcolony forms in the closed cell as the density remains low and the duration of the experiment is much less than the division time.

The experiments in either open or closed cells have been achieved with glass, PDMS 1/5, and PDMS 1/25 as a substrate, corresponding to hard, intermediate, and soft surfaces of a respective Young modulus of 5×10^3, 3.6, and 1 MPa. Details on the culture protocol and on the materials are provided in the appendices.

III. RESULTS

Figure 1 shows some micrographs taken in the open cell on the different surfaces after 8 days of growth, corresponding to the final time of the experiment of biofilm growth. The large black spots consist of microcolonies that result from the clustering of bacteria. The microcolonies contain a small number of cells, typically 10 at maximum. Smaller black dots are individual bacteria. Clearly, the soft surface PDMS 1/25 is covered by numerous clusters, while fewer are detected on the hard glass. Quantification of this effect is reported in Fig. 2(a) where the surface number density of microcolonies is plotted as a function of time. At early times all surfaces are covered by the same number of microcolonies that formed in suspension before the start of the experiment. At larger times, the number of microcolonies is nearly three times as large on the soft PDMS 1/25 than on the hard glass one.

The kinetics of cellular growth is, however, not dependent on the type of substrate as shown in Fig. 2(b) where the surface number density of bacteria $\rho(t)$ is plotted against time. We adjust $\rho(t)$ with the logistic equation $\rho(t) = \rho_i + \frac{\rho_\infty - \rho_i}{1+[(\rho_\infty-\rho_i)/\rho_i - 1]\exp[-(t-\lambda)/\tau_{\rm div}]}$, where $\rho_i = 2 \times 10^{-3}\mu{\rm m}^{-2}$ and $\rho_\infty = 11 \times 10^{-3}\mu{\rm m}^{-2}$ are the initial and the final number density of bacteria [23]. $\lambda = 3.2 \pm 0.4$ days defines a period of latency such that $\rho(\lambda) = 2\rho_i$, and $\tau_{\rm div} = 40 \pm 7$ hr is the division time.

For a given ρ, the various phenotypes shown in Fig. 1 should arise from specific surface dynamics, which we have studied in detail in the closed cell. The probability distribution functions of displacements (time interval $\Delta t = 100$ s), shown in Fig. 2(b) (inset), reveal marked peaks at distances smaller than the radius of the bacteria (lower bound $r_a \sim 1.4$ μm), indicating the presence of immobile cells. The broad tails characterize motile ones.

Analysis of the trajectories of motile bacteria on each type of surface (closed cell) shows that they evolve diffusively, with the ubiquitous intermittent "run" and "tumble" dynamics associated with identical caracteristic times $\langle\tau_r\rangle \sim 5$ s and $\langle\tau_t\rangle \sim 15$ s, leading to a diffusion coefficient $D \sim 0.05$ $\mu{\rm m}^2\,{\rm s}^{-1}$ as in Ref. [22]. Motile bacteria have the same dynamics whatever the substrate.

Figure 2(b) (inset) suggests that soft surfaces give rise to a higher number of unmotile bacteria n_u, as shown by the amplitudes of the peaks at small displacements. n_u is computed by tracking cells that do not travel a distance larger than 2 μm during $\Delta t = 100\,{\rm s} > \langle\tau_t + \tau_r\rangle$. The resulting proportion of motile bacteria $p_m = n_m/(n_m + n_u)$ amounts to $p_m = 0.9, 0.7,$

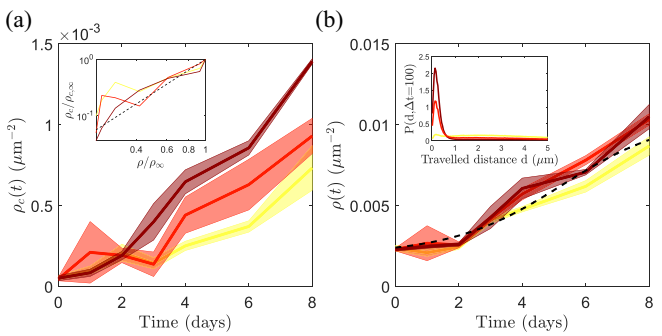

FIG. 2. (a) Number density of microcolonies as a function of time. From the darkest to the brightest line: PDMS 1/25, 1/5, and glass. Inset: logarithmic plot of the number of microcolonies as a function of ρ, with both axes rescaled by the final experimental value. Black dashed line indicates a slope 2. (b) Number of detected bacteria on the surface. Plain line: experimental results. Black dashed line: Logistic growth model, see text. Inset: probability density function of displacement of individual bacteria obtained in the closed cell. Color code identical for (a) and (b).

and 0.25 for the glass, PDMS 1/5, and 1/25, respectively. This leads to our main experimental result: microcolonies form preferentially on softer surfaces, corresponding to a low proportion of motile cells.

Modeling and numerical simulations

Experiments show that the clusters are not motile. Thus, we consider that attachment-detachment events involve only one single bacterium and a cluster. For simplicity, we disregard cell growth and consider homogeneous population for now. Let c_i be the surface number density of the clusters containing i cells and J_i the net rate at which the i clusters transform to $i+1$ ones. Following Ref. [24] we have $\dot{c}_i = J_{i-1} - J_i$ for $i \geqslant 2$ and $\dot{c}_1 = -2J_1 - \sum_{i=2}^{\infty} J_i$. The J_i are given by equations $J_i = a_i c_1 c_i - b_{i+1} c_{i+1}$, where a_i and b_i are kinetic coefficients ($[a] = L^2 T^{-1}$ and $[b] = T^{-1}$). This infinite system of differential equations forms the Becker-Döring discrete equations for a fragmentation-coagulation process with conservation of mass $\rho = \sum_{i\geqslant 1} i c_i = n/S = \text{const}$ [24,25].

Since the clusters contain only a few bacteria, we assume that the rate at which the cells bind to and are released from microcolonies is $a_i = i \times a$ and $b_i = i \times b$, respectively. We focus on the long time limit where $J_i = 0$ ($i \geqslant 1$). Then the solution of the recursive relations gives $c_i = \frac{1}{i}(\frac{a}{b})^{i-1}(c_1)^i$ from which $c_1 = \frac{\rho}{1+\chi\rho}$ where $\chi = a/b$. With $\sum_{i\geqslant 1} c_i = c_1 + \rho_c$ (ρ_c is the number density of clusters), we obtain $\rho_c = -\frac{1}{\chi}\ln(1-\chi c_1) - c_1$. In the limit $\chi\rho \ll 1$, the order of magnitude for $c_1 \sim \rho$ and combining the expression of ρ_c Taylor-expanded to second order yields

$$\rho_c \sim \frac{\chi}{2}\rho^2. \tag{1}$$

Let us emphasize that in this long time limit, ρ_c will not depend on transport as given by the average diffusion coefficient. The characteristic time of the coagulation-fragmentation process $t^\star \sim 1/(b + a\rho) \sim t_b = 100\,\text{s}$ (see below) provides a condition $\frac{\Delta n}{n} = \frac{t^\star}{n}\tau_{\text{div}}^{-1} \sim 10^{-6} \ll 1$ for the number of clusters reaching equilibrium before significant cell growth has occurred. The quadratic form (1) agrees satisfactorily with the results in Fig. 2(a) (inset), although the appearance of tridimensional growth after 8 days of experiments limits the relevance of the analysis to a timescale too short for evidencing of a proper scaling.

Akin to inert particles [26], we assume that each bacterium is surrounded by a "disk of influence" of radius d_a such that every bacterium entering this disk has a finite probability to stick. However, the interaction of between bacteria is different from inert colloids and we assume that it is driven by (type IV) pili-pili attachment, as in other similar systems [16,20]. Correspondingly, we consider that attachment and detachment events occur within well-defined characteristic timescales t_a and t_b, respectively. Then, dimensional analysis suggests $a \sim \pi d_a^2/t_a$ and $b \sim 1/t_b$. We now test this, together with Eq. (1), with numerical simulations.

As sketched in Fig. 3(a), the bacteria in the numerical simulations diffuse and interact according to the following rules: (1) only single bacteria can be motile (in proportion p_m), following Brownian motion with an effective diffusion coefficient D, (2) every particle entering the disk of influence of another one has a probability $p_{att} = \delta t/t_a$ to stick, where δt is the simulation step, and (3) every bound particle that can be motile (in proportion p_m) can detach with probability $p_{\text{det}} = \delta t/t_b$.

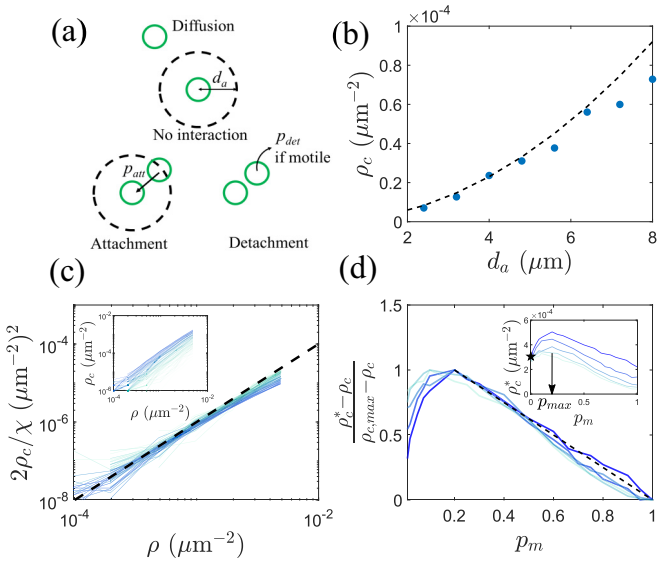

FIG. 3. Numerical simulations. (a) Sketch of the mechanism for attachment and detachment processes. (b) Number density of microcolonies versus d_a. Dashed line represents the model (1). Each point is the average of 10 runs. (c) Numerical results are rescaled with Eq. 1 (dashed line indicates a slope 2). Parameters $100 < t_a < 1000\,\text{s}$, $50 < t_b < 500\,\text{s}$, and $2 < d_a < 8\,\mu\text{m}$. Each curve is averaged over four runs. Darker curves correspond to higher values of $\chi = \pi d_a^2 t_b/t_a$. Inset: ρ_c as a function of ρ before rescaling. (d) Inset: final number of microcolonies with heterogeneous motility ρ_c^*, as a function of p_m [same color code as (c)]. The star indicates theoretical predictions considering a Rayleigh-distributed interparticle distance (see text). Main graph: rescaled number of microcolonies as a function of p_m. The black dashed line indicates the fit by $(1-p_m)/(1-p_{\max})$ for $p_m > p_{\max}$.

We start with the simplest case where the proportion of motile bacteria $p_m = 1$ and take an order of magnitude for $t_b \sim t_a \sim 100\,\text{s}$ [16,17,27]. As shown in Fig. 3(b), the number density of microcolonies ρ_c from simulations follows Eq. (1) when d_a varies, with $\chi = a/b = \pi d_a^2 t_b/t_a$ and the restriction $r_a < d_a < 1/\rho^{1/2}$ since the radius of the disk of influence shall be much smaller than the average interparticle distance. Moreover, Fig. 3(c) indicates that simulations match the scaling Eq. (1) for a broad range of particle densities and characteristic times t_a and t_b.

Then we plot in Fig. 3(d) (inset) the number density of microcolonies ρ_c^* for different levels of heterogeneity as obtained from various proportions of motile bacteria p_m. Numerical results agree with the experimental data qualitatively and fewer microcolonies are obtained with the high proportion of motile bacteria. When no particle is motile ($p_m = 0$), the interaction is possible only if two cells are situated within the radius of influence d_a. Assuming that cells are located randomly on the surface, the distance to the closest neighbor is distributed with a Rayleigh law [28], with parameter $\sigma = 1/\sqrt{2\pi\rho}$. Accordingly, the cumulative distribution function

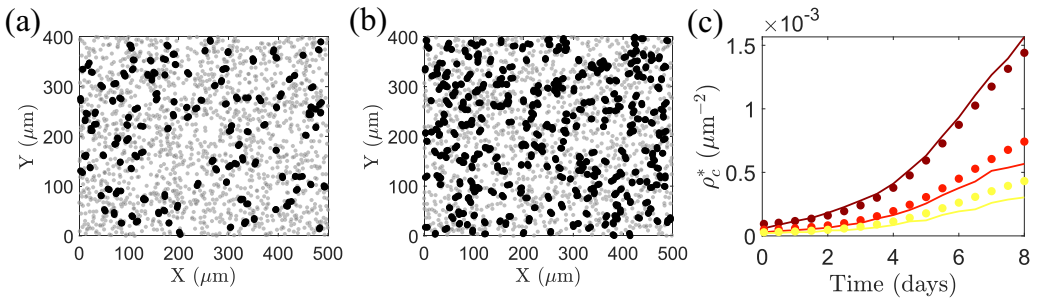

FIG. 4. Simulations with bacterial growth, run with $d_a = 3\ \mu$m, $t_a = 450$ s, and $t_b = 100$ s. (a) and (b) Colonization maps at long times, on a "high-motility" and a "low-motility" surface, defined with $p_m = 0.7$ and 0.25, respectively. Unbound cells are in light gray; and attached ones are in black. (c): Number of detected microcolonies as a function of time for $p_m = 0.9$, 0.7, and 0.25. Lines: simulation results. Dots: Eq. (2). Darkest lines correspond to lowest motilities.

gives $p_{d\leqslant d_a} = 1 - \exp[-d_a^2/(2\sigma^2)]$ and a number of pairs $\sim p_{d\leqslant d_a} \times \rho/2$ [star in the inset Fig. 3(d)]. For $p_m = 1$, $\rho_c^* = \rho_c$ as given by Eq. (1) and shown in Fig. 3(d). In between, ρ_c^* reaches a maximum $\rho_{c,\max}$ at a given motility $p_{\max} \sim 0.2$ common to all simulations [Fig. 3(d) (inset)]. Thorough numerical investigation of the maximum shows that $\rho_{c,\max} - \rho_c \sim 1/2\pi d_a^2 \rho^2$ and linear extrapolation between $\rho_{c,\max}$ and ρ_c [Fig. 3(d)] provides the final result for the surface number density of microcolonies for different amounts of motility:

$$\rho_c^* \sim \frac{1}{2}\pi d_a^2 \left[\frac{t_b}{t_a} + \frac{1-p_m}{1-p_{\max}}\right]\rho^2, \qquad (2)$$

which is valid for $p_m > p_{\max}$, relevant for our experiments. The first term in the brackets corresponds to Eq. (1), while the second one provides influence of motility. In Eq. (2), t_a, t_b, and d_a describe cell-cell interactions, while p_m stands for the degree of heterogeneity of the motility, whose relation with cell-substrate interactions for the present study is discussed below. Above the timescale $\tau = \lambda + \tau_{\text{div}} \log[\mathcal{S}/(N_i\,\pi\,d_a^2)] \sim 8$ days, with $\mathcal{S} = 2 \times 10^5\ \mu$m^2 the surface area onto which initially $N_i = 400$ particles are present, we expect tridimensional growth to dominate biofilm growth.

Data analysis consistently show that for $10 < \chi < 100\ \mu$m^2, a variation of p_m from 0.2 to 1 increases the ratio of attachment and detachment events of 20%. While this effect deserves further theoretical investigations, this clearly highlights that enhanced motility favors the escape of bacteria from microcolonies. This is the main mechanism responsible for the lower number of microcolonies on hard surfaces.

Now we set $d_a = 2\,r_a \sim 3\ \mu$m for the order of magnitude of the interaction length. A measure of the detachment time $t_b \sim 100$ s can be obtained from experiments by the analysis of the video recorded in the closed cell, by detecting some detachment events and counting the time elapsed between attachment and detachment of two individual bacteria. Using Eq. (2) with the experimental data for (p_m, t_b) and the estimate for d_a mentioned above provides a consistent characteristic time for attachment $t_a = 450 \pm 150$ s whatever the surface. This is compatible with the order of magnitude found for different bacteria with type IV pili [16,17] and could suggest an ubiquitous interaction mechanism for bacteria displaying hairlike appendages. Our model suggests that the nature of the substrate affects only motility and not cell-cell interactions.

Finally, we show in Figs. 4(a) and 4(b) the morphologies obtained at long times from full simulations on "high-motility" and "low-motility" surfaces ($p_m = 0.7$ and 0.25, respectively) where bacterial growth is taken into account as described by the Logistic equation [Fig. 2(b)] (see the appendices for the details). Consistent with experiments, small and sparse microcolonies are obtained, with more clusters on the "low-motility" surface. Figure 4(c) displays the similar temporal evolutions of the number of microcolonies from both the simulations and model (2), showing agreement.

IV. DISCUSSION

What is the mechanism responsible for the different fraction of motile bacteria (i.e., heterogeneity) on the various surfaces? To gain further insights, we have submitted, after 3 days of experiments of growth, some samples to a high flux of deionized water and found that the amount p_{rins} of remaining microcolonies is inversely correlated to the Young modulus (see the appendices). Since the two PDMS samples have the same surface energy, physico-chemical effects are not relevant, and this shows that adhesion is enhanced by the softness of the surface. This basic result suggests an intuitive correlation between adhesion and the dynamical arrest observed on soft surfaces.

The model is built at the particle scale, and its parameters stand for unknown processes at a molecular scale. While it is clear that the type IV pili play a key role in bacterial adhesion [29–32], their complex interactions with surfaces and with other bacteria deserve to be studied extensively with, for example, mutants of a variable number of pili or surfaces of controlled structure. The description proposed here does not, however, rely upon explicit cell-substrate or cell-cell adhesion mechanisms.

We show that strong interactions with the surface provides a high level of heterogeneity. Such heterogeneity [33] is key in maintaining the integrity of the biofilm of other bacteria [34], in immune evasion [35], and in some metastatic processes [36]. This suggests that the relevance of heterogeneous phenotypes among a given strain may be a generic feature of active matter whose emergence shall be further investigated.

V. CONCLUSIONS

We have observed that microcolonies grow preferentially on soft surfaces. This is due to the increased adhesion, giving

rise to a high proportion of nonmotile bacteria which cannot escape microcolonies. The order of magnitude of the number of microcolony is well described by a kinetic model with a correction for the proportion of motile bacteria. Understanding how adhesion strength and heterogeneous dynamics are linked could be useful to the implementation of new strategies for limiting the virulence of pathogens.

ACKNOWLEDGMENTS

This work was carried out with partial financial support of the Université Sorbonne Paris Cité in the framework of the Programme Interdisciplinaire des Energies de Demain. The authors would like to thank F. Chauvat, M. Jarrahi and J.-P. Thermeau for useful discussions and A. Méjean for kind help regarding the culture of the cyanobacteria.

APPENDIX A: EXPERIMENTAL DETAILS

1. Materials

The wild-type strain of the cyanobacterium *Synechocystis* sp. PCC 6803 is cultured in a BG11 standard mineral medium. Cell suspensions are placed under a white light of intensity of 1.3 W m^{-2} for 7 days and then kept in the dark for 24 hours. The suspensions are finally left for 2 hours under ambient light until starting an experiment. This protocol results in a homogeneous cellular behavior on glass [22].

The surfaces on which microcolony grow are glass (contact angle with water $\theta \sim 60^\circ$) and two different polydimethylsiloxanes (PDMS, Sylgard 184, Dow Corning) prepared with ratios of curing agent/polymeric base of 1/5 and 1/25 and for which $\theta \sim 100^\circ$.

The growth of microcolonies is studied in an "open cell" made of a Petri dish covered with a lid into which a small 1 mm hole is drilled, ensuring gas exchange throughout the 8 days of the experiment. First, samples of the different surfaces are placed together at the bottom the cell. The cell is then filled with the bacterial suspension, the lid is sealed, and the system is placed inside an incubator with white light (1.3 W m^{-2}). The imaging setup, based on a standard microscope, is placed in the incubator to record images of each surface. Images ($400 \times 500\,\mu m^2$) are then processed as explained in the main text.

Because of convection, the diffusive dynamics of the bacteria cannot be characterized conveniently in the open cell. We then used a previous configuration in a closed cell as in Ref. [22]. The dynamics on the hard glass surface is studied on the bare glass slide while for the soft and intermediate surfaces, millimetric droplets of PDMS are deposited on the glass slide and let to cure for 2 days at room temperature (only one substrate at a time can be studied with this setup). A droplet of suspension is then deposited on the glass slide and trapped with a glass cavity. This cell is sealed with grease and contains a small volume of liquid, thus totally suppressing convection. After 1 hour at rest so that sedimentation is complete, the motion of the bacteria is video recorded and analyzed by particle tracking [22].

2. Probing adhesion

To get a rough estimate of the interactions between the bacteria and the surfaces, some open cells were thoroughly washed after 3 days of growth, by submitting the substrates to a high tangential flux of deionized water, thus detaching some microcolonies. Image analysis of the washed surfaces provides the number of remaining bacteria from which the proportion of attached cells p_{rins} is deduced. We found $p_{\text{rins}} =$ 44%, 56%, and 63% $\pm$ 5% for the glass, PDMS 1/5, and PDMS 1/25, respectively.

3. Microcolony formation and detection

In order to detect the microcolonies on a surface, we start from raw images to which we apply a bandpass filter with ImageJ. The background of each image is subtracted before inversion and binarization. Microcolonies are detected on a size criterion: groups of pixel containing less than 80 units (30 μm^2, corresponding to an effective radius of 3.1 μm) are ignored. The number of remaining clusters defines the number of microcolonies. Data are averaged over four different images.

4. Computation of the average number of bacteria on each surface

We have determined the number of bacteria n_{frame} on a given image by summing the floor function of the area of each detected cluster divided by the area of an average particle $\mathcal{A}_b = \pi r_b^2 = 15\,\mu m^2$. If the floor function is less than 1 we set the value to 1. Spots smaller than 16 pixels ($\pi r_a^2 = 6.2\ \mu m^2$) are considered as artifacts and are removed from the analysis. This is summed up by Eq. (A1), where P bacteria of size $\mathcal{A}_i \geqslant 16$ pixels are detected:

$$n_{\text{frame}} = \sum_{i=1}^{P} \max\left[1, \text{floor}\left(\frac{\mathcal{A}_i}{\mathcal{A}_b}\right)\right]. \tag{A1}$$

We have repeated this procedure on four different areas of each surface. The number of detected bacteria $n(t)$ is defined as the average value of n_{frame} taken on these four images at time t.

APPENDIX B: NUMERICAL SIMULATIONS

Different types of motility are taken into account given the experimental proportion of motile bacteria p_m, and we consider that motile bacteria have the same behavior overall, as suggested by the experiments in the closed cell.

We define by n_i the number of cells for the simulation, randomly placed on a domain of size $\mathcal{S} = 2 \times 10^5 \mu m^2$ with periodic boundary conditions, resulting in a particle number density $\rho = n/\mathcal{S}$. A fraction $1 - p_m$ of these cells are set nonmotile and thus unable to move or detach. The other ones perform random Brownian motion with an effective diffusion coefficient $D = 0.05\ \mu m^2\ s^{-1}$, as in experiments. During the diffusion of a particular bacteria, a random number between 0 and 1 is computed if a neighbor is found at a distance $d < d_a$. If the random number is less than $p_{att} = \delta t / t_a$, then the cells bind to each other. The process is repeated for each particle

found at a distance less than d_a. $\delta t = 1$ s is the time step for the simulations, such that $\delta t \ll \min(t_a, t_b)$. Motile bacteria can detach from their neighbors with a probability $p_{\text{det}} = \delta t / t_b$ and then restart their diffusive motion.

To account for cellular growth as in Fig. 4, the number of simulated bacteria $\rho(t)$ is imposed the experimental logistic equation. The integer part $\mathcal{N}(t)$ of $n(t) = \rho(t)\mathcal{S}$ is computed, and a new particle is created and randomly placed if $\mathcal{N}(t + \delta t) > \mathcal{N}(t)$. At the end of the simulation, we consider as "microcolonies" bacterial aggregates that contain at least two bacteria. Data shown in Fig. 4(c) are obtained with $d_a = 3\ \mu$m, $t_a = 450$ s, and $t_b = 100$ s.

[1] B. Linse and S. Linse, Mol. BioSyst. **7**, 2296 (2011).
[2] T. Kiørboe, Scienta Marina **65**, 57 (2001).
[3] P. Michel, W. Benz, P. Tanga, and D. C. Richardson, Science **294**, 1696 (2001).
[4] A. Kumar, A. Alam, M. Rani, N. Z. Ehtesham, and S. E. Hasnain, Int. J. Med. Microbiol. **307**, 481 (2017).
[5] L. R. Thurlow, M. L. Hanke, T. Fritz, A. Angle, A. Aldrich, S. H. Williams, I. L. Engebretsen, K. W. Bayles, A. R. Horswill, and T. Kielian, J. Immunol. **186**, 6585 (2011).
[6] T. Bjarnsholt, APMIS Supp. **121**, 1 (2013).
[7] M. Planchon, T. Jittawuttipoka, C. Cassier-Chauvat, F. Guyot, A. Gelabert, M. F. Benedetti, F. Chauvat, and O. Spalla, J. Colloid Interface Sci. **405**, 35 (2013).
[8] R. M. Landry, D. An, J. T. Hupp, P. K. Singh, and M. R. Parsek, Mol. Microbiol. **59**, 142 (2006).
[9] M. Alhede, K. N. Kragh, K. Qvortrup, M. Allesen-Holm, M. van Gennip, L. D. Christensen, P. Ø. Jensen, A. K. Nielsen, M. Parsek, D. Wozniak, S. Molin, T. Tolker-Nielsen, N. Høiby, M. Givskov, and T. Bjarnsholt, PLoS ONE **6**, e27943 (2011).
[10] E. Ben-Jacob, I. Cohen, and H. Levine, Adv. Phys. **49**, 395 (2000).
[11] M. Klausen, M. Gjermansen, J.-U. Kreft, and T. Tolker-Nielsen, FEMS Microbiol. Lett. **261**, 1 (2006).
[12] M. E. Cates and J. Tailleur, Annu. Rev. Condens. Matter Phys. **6**, 219 (2015).
[13] G. S. Redner, M. F. Hagan, and A. Baskaran, Phys. Rev. Lett. **110**, 055701 (2013).
[14] M. C. Duvernoy, T. Mora, M. Ardré, V. Croquette, D. Bensimon, C. Quilliet, J. M. Ghigo, M. Balland, C. Beloin, S. Lecuyer, and N. Desprat, Nat. Commun. **9**, 1120 (2018).
[15] C. A. Weber, Y. T. Lin, N. Biais, and V. Zaburdaev, Phys. Rev. E **92**, 032704 (2015).
[16] D. Bonazzi, V. Lo Schiavo, S. Machata, I. Djafer-Cherif, P. Nivoit, V. Manriquez, H. Tanimoto, J. Husson, N. Henry, H. Chaté, R. Voituriez, and G. Duménil, Cell **174**, 143 (2018).
[17] J. Taktikos, Y. T. Lin, H. Stark, N. Biais, and V. Zaburdaev, PLoS ONE **10**, e0137661 (2015).
[18] R. D. Acemel, F. Govantes, and A. Cuetos, Sci. Rep. **8**, 5340 (2018).
[19] W. K. Smits, O. P. Kuipers, and J.-W. Veening, Nat. Rev. Microbiol. **4**, 259 (2006).
[20] E. R. Oldewurtel, N. Kouzel, L. Dewenter, K. Henseler, and B. Maier, eLife **4**, e10811 (2015).
[21] W. Pönisch, K. B. Eckenrode, K. Alzurqa, H. Nasrollahi, C. Weber, V. Zaburdaev, and N. Biais, Sci. Rep. **8**, 1 (2018).
[22] T. Vourc'h, H. Peerhossaini, J. Léopoldès, A. Méjean, F. Chauvat, and C. Cassier-Chauvat, Phys. Rev. E **97**, 032407 (2018).
[23] M. H. Zwietering, I. Jongenburger, F. M. Rombouts, and K. van 't Riet, Appl. Environ. Microbiol. **56**, 1875 (1990).
[24] O. Penrose, Commun. Math. Phys. **124**, 515 (1989).
[25] R. Becker and W. Döring, Ann. Phys. **416**, 719 (1935).
[26] S. Chandrasekhar, Rev. Mod. Phys. **15**, 1 (1943).
[27] V. Zaburdaev, N. Biais, M. Schmiedeberg, J. Eriksson, A. B. Jonsson, M. P. Sheetz, and D. A. Weitz, Biophys. J. **107**, 1523 (2014).
[28] S. Torquato, B. Lu, and J. Rubinstein, J. Phys. A: Math. Gen. **23**, 103 (1990).
[29] C. Berne, C. K. Ellison, A. Ducret, and Y. V. Brun, Nat. Rev. Microbiol. **16**, 616 (2018).
[30] J. D. Valentin, X.-H. Qin, C. Fessele, H. Straub, H. C. van der Mei, M. T. Buhmann, K. Maniura-Weber, and Q. Ren, J. Colloid Interface Sci. **552**, 247 (2019).
[31] K. C. Dansuk and S. Keten, Soft Matter **14**, 1530 (2018).
[32] C. A. Rodesney, B. Roman, N. Dhamani, B. J. Cooley, P. Katira, A. Touhami, and V. D. Gordon, Proc. Nat. Acad. Sci. USA **114**, 5906 (2017).
[33] T. Vissers, A. T. Brown, N. Koumakis, A. Dawson, M. Hermes, J. Schwarz-Linek, A. B. Schofield, J. M. French, V. Koutsos, J. Arlt, V. A. Martinez, and W. C. Poon, Sci. Adv. **4**, eaao1170 (2018).
[34] S. M. Horne, J. Sayler, N. Scarberry, M. Schroeder, T. Lynnes, and B. M. Prüß, BMC Microbiol. **16**, 262 (2016).
[35] M. W. Harman, S. M. Dunham-Ems, M. J. Caimano, A. A. Belperron, L. K. Bockenstedt, H. C. Fu, J. D. Radolf, and C. W. Wolgemuth, Proc. Nat. Acad. Sci. USA **109**, 3059 (2012).
[36] G. A. Franzetti, K. Laud-Duval, W. Van Der Ent, A. Brisac, M. Irondelle, S. Aubert, U. Dirksen, C. Bouvier, G. De Pinieux, E. Snaar-Jagalska, P. Chavrier, and O. Delattre, Oncogene **36**, 3505 (2017).